CHALMERS UNIVERSITY OF TECHNOLOGY
SE - 412 96 Gothenburg, Sweden
Telephone: + 46 - (0)31 772 10 00
www.chalmers.se

CHALMERS

PEIGANG LI Experimental Study on Cold Lap Formation in Tandem Gas Metal Arc Welding 2011

Experimental Study on Cold Lap Formation in Tandem Gas Metal Arc Welding

PEIGANG LI

Department of Materials and Manufacturing Technology
CHALMERS UNIVERSITY OF TECHNOLOGY
Gothenburg, Sweden 2011

THESIS FOR THE DEGREE OF LICENTIATE OF ENGINEERING

Experimental Study on Cold Lap Formation in Tandem Gas Metal Arc Welding

PEIGANG LI

Department of Engineering Science
UNIVERSITY WEST
TROLLHÄTTAN, SWEDEN 2011

CHALMERS

Department of Materials and Manufacturing Technology
CHALMERS UNIVERSITY OF TECHNOLOGY
GOTHENBURG, SWEDEN 2011

Experimental Study on Cold Lap Formation in Tandem Gas Metal Arc Welding

Peigang Li

Technical Report no 69/2011.
ISSN: 1652-8891

Department of Materials and Manufacturing Technology
Chalmers University of Technology
SE-412 96 Gothenburg, Sweden Tel: +46 (0)31-772 1000.

Printed by Chalmers Reproservice
Gothenburg, Sweden 2011

To Xiaolin and my coming baby

Abstract

Tandem gas metal arc welding (GMAW) is a high productivity welding process which is applied in many industries. However, a type of imperfection, known as cold lap, was revealed that mostly accompanies the tandem GMAW process.

Cold lap is a small lack of fusion in size at the weld toe which can have a negative influence on the fatigue life of the weld [1, 2]. It generally runs parallel to the surface of the parent plate. Due to its small size, it has not been successful to detect cold lap by any non-destructive test (NDT) method. With a lot of work, it has been noticed that it is hard to produce a weld without cold laps. Even for some post-treatment methods, e.g. TIG-dressing, cold lap cannot be eliminated completely [2]. Therefore, a better understanding of the formation mechanism is required to be able to avoid their formation.

The main objectives of this thesis are to classify cold laps, to characterise cold lap interfaces, and to investigate the main influencing factors on cold lap formation. For this purpose, several series tandem GMAW experiments were performed. Domex 355 MC was used as the base metal and OK Autrod 12.51 Φ 1.2 was used as the consumable material. Different shielding gases (pure argon and pure carbon dioxide) and surface conditions (blasted surface and milled surface) of the base metal were applied. A sealed chamber was used in the experiment to ensure a non-oxidising or oxidising welding environment. Cross sections of the cold laps were prepared by a conventional metallographic method, e.g. cutting, mounting, polishing, and etching (if necessary). The metallographic samples were evaluated with the help of both a light optical microscope and a scanning electron microscope (SEM) with an attached energy dispersive spectroscopy (EDS). Also, the interface between spatter and base metal was investigated using the same method as an assistant study of cold laps.

The results showed three types of cold laps, i.e. spatter cold lap, overlap cold lap, and spatter-overlap cold lap. The cold lap is mostly composed of voids and oxides. For the materials (welding consumables and parent materials) used in the experiments, the oxides were shown to be manganese-silicon oxides (Mn-Si oxides). It was also found that Mn-Si oxides have a significant influence on the occurrence of overlap cold lap. The blasted surface condition can have a minor effect on enhancing cold laps. By studying the spatter/base metal interface, it is believed that temperature/energy are the other important factors for the formation of cold laps.

Keywords: tandem GMAW, cold lap, imperfection, lack of fusion, spatter, overlap, overflow, manganese, silicon, oxides, temperature/energy.

Acknowledgements

In my studies I have had a lot of help from many people. First of all, I would like to express my deep gratitude to my main supervisor Professor Lars-Erik Svensson for his patience, discussions, suggestions, and help. I also would like to give my sincere thanks to my ex-main supervisor Professor Per Nylén for his valuable encouragement. My sincere thanks are due to my assistant supervisor Nicolaie Markocsan for his positive advice and frank discussion. Special thanks to my examiner Professor Uta Klement for her efforts to push my PhD study forward.

My heartfelt thanks go to Professor Bill Lucas, Professor Yoshinori Hirata, and Dr. Stephan Egerland for their valuable comments, helpful discussions and faithful advice during the IIW conference and events. Many people have given me support and deserve my thanks: Dr. Niklas Järvstråt, Associate Professor Håkan Wirdlius, Mr.Tore Ronnhult, Professor Nils Stenbacka, Dr. Yiming Yao, Mr. Hasse Olsson, Associate Professor Kenneth Hamberg, Mr. Peter Nerman, Mr. Joakim Hedegård, Mr. Kjell-Arne Persson, Mr. Lars Hammar, and Mr. Nicolas Curry. I thank all my colleagues who helped to create an inspiring and more interesting working environment. Without the financial support from the LOST and WIQ projects, this work would not have been possible. Also, I would like to thank Volvo Construction Equipment (VCE) for important support.

Finally, I would like to dedicate all of my love and this work to my wife, Xiaolin Su, and my coming baby. You mean the world to me!

Trollhättan, June 2011

Peigang Li

Abbreviations and notations

Abbreviations /notations	Description
Al	Aluminium
Ar	Argon
ASM	American Society for Metals
BSE	Back Scatter Electron
C	Carbon
Co	Cobalt
CO	Carbon monoxide
CO_2	Carbon dioxide
Cr	Chromium
CTWD	Contact Tip Working Distance
EDS	Energy Dispersive Spectroscopy
Fe	Iron
GMAW	Gas Metal Arc Welding
Larc	Arc Length
MAG	Metal Active Gas
Mg	Magnesium
MIG	Metal Inert Gas
Mn	Manganese
MnO	Manganese oxide
MnS	Manganese sulphur
Mo	Molybdenum
N	Nitrogen
Nb	Niobium
NDT	Non-Destructive Test
Ni	Nickel
RLoF	Ratio between the length of lack of fusion at the interface and the entire length of the spatter/base metal interface
SE	Secondary Electron
SEM	Scanning Electron Microscopy
Si	Silicon
SiO	Silicon monoxide
SiO_2	Silcon dioxide
SMAW	Shielded Metal Arc Welding
STEDV	Standard Deviation
TA	Troch Angle
Ti	Titanium
TIG	Tungsten Inert Gas
TS	Travel Speed
V	Vanadium
VCE	Volvo Construction Equipment
WFS	Wire Feed Speed

WireC	Wire Combination
WS	Welding Speed
VT	Visual Test
Zr	Zirconium

Contents

1 Introduction

1.1 Background

This thesis contributes towards the fundamental understanding of the formation of cold lap, which is a type of welding defect, to be explained later.

Welding is very important in modern manufacturing industry. Gas Metal Arc Welding (GMAW) is especially utilized in offshore industry and vehicle manufacture due to its high welding productivity. It is well known that some imperfections generated in the GMAW process, such as pores, inclusions, undercuts, etc, are inevitable in civil industrial manufacture. These imperfections can influence the properties of the welded structures, especially the fatigue properties. Fatigue is a local phenomenon in which the local stress level and/or local defects can influence the service life of the materials severely. The fatigue properties of the welded structures always need to be improved for the development of new products, which must usually feature increased load capacity, higher travel speeds and longer life. Since the last century, many fatigue tests have been performed and evaluated on welded samples using different welding methods, filler materials, parent materials, welding parameters, shielding gases, joint types, and fatigue loadings [1-6]. Besides weld geometry, cold lap was revealed as another important factor which can have a detrimental effect on the fatigue life of the welded structures. Recently, a new corporate standard was developed within Volvo Construction Equipment (VCE), in which cold lap was firstly given and related to different quality classes[7].

However, very limited knowledge about cold lap is available in literature. Even the detection of cold lap is an obstacle for studying it. Previous investigations have shown that it is very difficult to produce a weld without cold lap when using GMAW. Therefore, it is important to understand cold lap fundamentally, e.g. classification, characterisation, mechanism of formation, etc.

1.2 Objective

The objective of this ongoing work is to study cold laps in order to better understand the phenomena behind their formation and the mechanisms involved. First, a classification of cold laps is given. Physical characterisation of the cold lap interface is a second important part of this thesis. Thirdly, the factors that are supposed to have a significant influence on cold lap formation are presented. Regarding the welding process, different influence factors are illustrated to explain the cold lap formation.

1.3 Limitations

In this study, the detection of cold laps has continued to be an obstacle. Since cold laps are small in size, all standard NDT (Non-Destructive Test) methods have failed in detecting them, and only visual tests (as a preliminary test) and destructive tests were found to be efficient and reliable methods.

Blasted surfaces of the base materials have been broadly introduced in industry. Therefore, this study only focuses on blasted or burr grinding surface conditions.

According to previous studies, the solid wire can give the highest frequency of cold lap in the welding process. One type of both welding filler material (solid wire) and base metal were used in this study.

Only two types of joint were used in this study, i.e. butt joint and bead-on-plate, to reduce the uncertainties of the welding process. Tandem GMAW was selected as the welding process in this study since it was mostly applied in the workshop of VCE.

It is also important to point out that the cold laps discussed in this thesis only refer to 'local' cold laps, which are compared with a type of cold lap due to a lack of fusion along the entire weld toe in the longitudinal direction. Usually, the cold laps along the entire weld toe are due to 'incorrect' welding setup or a very thick oxide layer on the base metal surface. Therefore, it is believed that the cold lap along the entire weld can be easily avoided in the modern GMAW process.

2 GMAW process

Gas Metal Arc Welding (GMAW) refers to an arc welding process using an arc between a continuously filling electrode and the welding pool with a shielding gas. GMAW was introduced in the 1920s, but it was not until 1948 that it was made commercially available. When using different shielding gases, GMAW is also called MIG (Metal Inert Gas)/MAG (Metal Active Gas) if the shielding gas is an inert or active gas. In Europe the process is also simply called MIG welding. The use of GMAW can bring many advantages. It can be used for almost all commercial metals and alloys; it can be done in all positions; continuous wire feeding is possible; deposition rates are significantly high; it is easy to automate welding; and minimal post-weld cleaning is required. Therefore, GMAW is utilized broadly in industry.

The typical equipments for GMAW include power source, wire supply reel, wire feeding drive rollers, flexible conduit, hose package, welding gun, contact tube, gas nozzle, and shielding gas, etc [8].

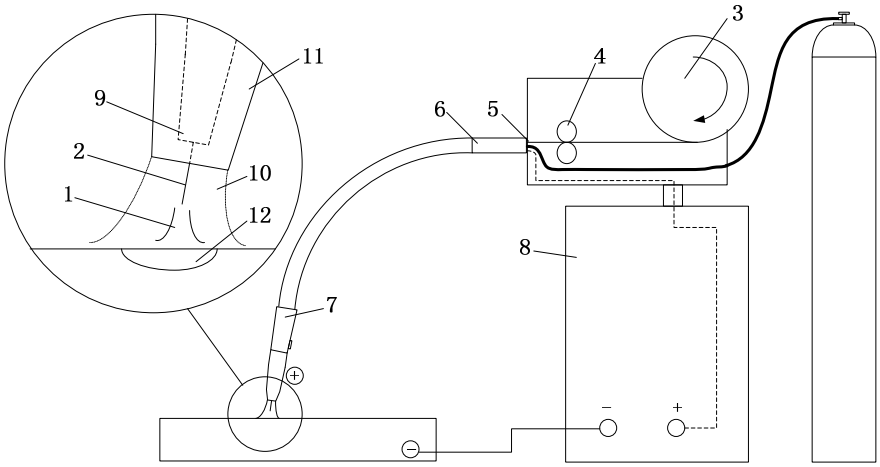

Figure 1 Typical GMAW equipment. (1: Arc; 2: Metal wire electrode; 3: Wire supply reel; 4: Wire feeding drive rollers; 5: Flexible conduit; 6: Hose package; 7: Welding gun; 8: Power source; 9: Contact tube; 10: Shielding gas; 11: Gas nozzle; 12: Weld pool.) (Adapted from [8])

The GMAW welding process is dependent on a number of welding parameters, the most common variables being [8]:

- Electrode diameter
- Voltage
- Wire feed speed and current
- Welding speed
- Electrode stick-out
- Choice of shielding gas and gas flow rate
- Torch and joint position

To ensure good welding performance, most of these parameters must be optimized and matched to each other. The working point must be within the working range or tolerance box for the particular welding situation. Generally, the size of electrode is chosen according to the welding current. When a higher welding current is used, an electrode with a higher diameter should be chosen. Regarding voltage, increased voltage increases the arc length and gives a

wider weld bead. But too high a voltage will bring the risk of undercut. If short arc welding is used, a higher voltage reduces the short circuit frequency, which will give larger drops and more spatter. On the other hand, too low a voltage will increase the risk of stubbing and poor start performance. Normally the voltage should be set for a stability arc. For GMAW, the current is set indirectly by the wire feed speed and diameter. Current is the main parameter for welding to achieve sufficient welding penetration. However, it is also important to strike a balance with welding speed, voltage with respect to the arc stability, and weld quality. When setting welding speed, this also has a considerable effect on the shape and penetration of the weld. Therefore, a higher welding speed always accompanies higher current and voltage and may result in poor stability. Electrode extension, also called stick-out, refers to the distance from the contact tip to the melted electrode tip. Practically, it is easy to use the distance from the contact tip to the workpiece (CTWD) to express electrode extension. The relationship between stick-out, CTWD and arc length is shown in Figure 2. Too small a stick-out increases the risk of burn-back, where the arc will weld the electrode together with the contact tip. Too long a distance will increase the risk of stubbing, especially at the start. The contact tip-to-work distance also has an influence on the current and penetration profile. If the electrode extension is increased, the current and heat input decrease while the amount of deposited metal remains the same. This reduces the penetration, and even if it was unintentional a risk of a lack of fusion arises. Therefore, the stick-out is usually kept constant during the welding operation. Torch angles relative to the joint are also an important welding parameter. If the torch/wire is directed away from the finished part of the weld (forehand technique), this makes the penetration profile more shallow and the width of the seam wider. On the other hand, if it is directed towards the finished part of the weld (backhand technique), the penetration will be deeper and the seam width will be narrower [8-10].

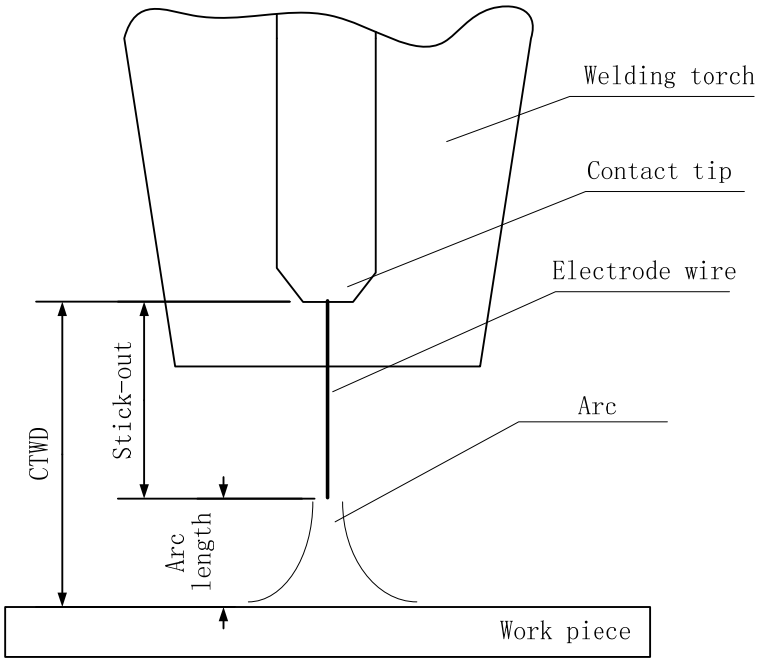

Figure 2 Relationship between stick-out, CTWD and arc length in GMAW

Solid wires and cored wires are the two types of wires used in GMAW. The latter type consists of a metallic outer sheath, filled with flux or metal powder. The flux cored wires can have either a rutile or basic filling. They can also be self-shielded for use without shielding gas. The cost per

unit of cored wires is considerably higher than that of solid wires, but they are in some respects superior to solid wires. A high deposition rate and good side wall penetration are features of cored wires. Basic flux cored wires have similar performance to basic manual stick electrodes, giving a tough and crack resistant weld metal [8]. Generally, the size of the electrode used for GMAW is smaller compared with that used for submerged arc and manual stick electrode welding. The wire is usually 0.9 mm to 1.6 mm in diameter [9].

For GMAW, the stability of the arc depends largely on how the molten metal is transferred in the arc. One can distinguish essentially between two different types of arcs, depending on the material transport: the spray arc and the short arc (short-circuiting arc) [8, 9].

Tandem GMAW is regarded as a type of high efficiency GMAW welding process in which higher welding speed can be obtain by using the double wire. In tandem GMAW, two individual wires are melted into one common weld pool using two arcs, as shown in Figure 3. Two power units are used for the wires. Therefore, the welding parameters for each wire can be set completely individually. However, because the two arcs are very close to each other, it is much more complicated and difficult to set the welding current and voltage for each wire. An incorrect welding parameter setting will increase the risk of interference between the two arcs through magnetic arc blow effect.

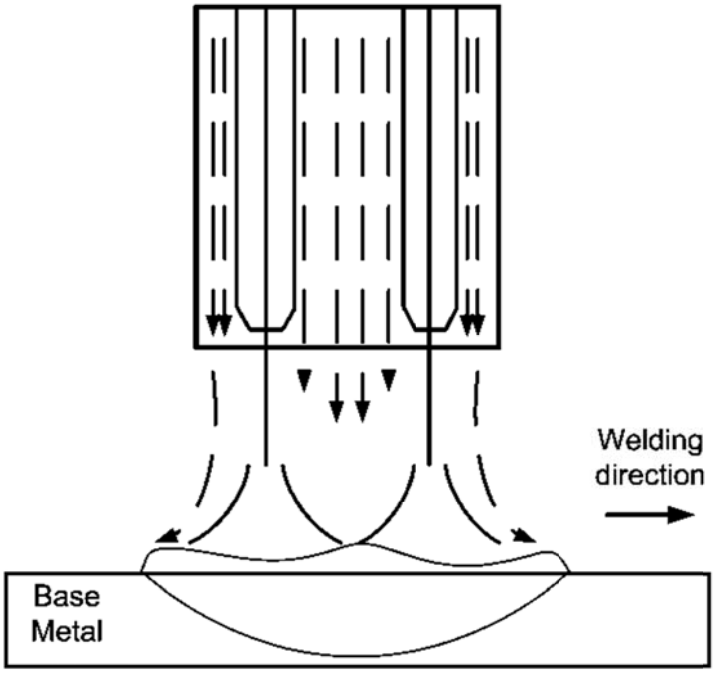

Figure 3 Tandem GMAW with two individual wires and arcs

Moreover, due to an additional wire being introduced into the welding process, more welding parameters need to be set for the tandem GMAW, e.g. the angle between the two wires, the distance between the wires, and the ratio of current and voltage between the two wires.

3 Cold laps

Cold lap is a relatively new word to describe an imperfection at the weld toe. The imperfection was first discovered in the 1990s during experimental work to improve the fatigue properties of welds. It was also observed at that time that cold laps can have an important influence on the fatigue life of the welded structures. However, in terms of available literature, there are a limited number of publications presenting studies on weld process influence on cold lap formation or phenomena which promote cold laps. In this chapter, the few available articles are summarized in order to give a brief overview of cold laps.

3.1 Definition of cold laps

In this thesis, cold lap refers to a crack-like imperfection at the weld toe which has a negative influence on the fatigue properties of the weld.

The cold lap was found in fatigue tests carried out by Lopez Martinez and Korsgren [1] in the 1990s . In their fatigue investigation, two welding methods were evaluated, i.e. Shielded Metal Arc Welding (SMAW) and Gas Metal Arc Welding (GMAW). The welding runs were performed in the best welding position (1G). Four different types of welding consumable materials were involved: OK 48.00, a basic coated electrode; PZ6130, a basic flux cored wire; PZ6111, a rutile flux cored wire; and OK 12.51, a solid wire. For GMAW, two types of shielding gases were applied in the welding experiments. Different welding parameters, i.e. welding current, welding voltage, and interpass temperature, were used due to the different methods and different diameters of the electrodes. The details are shown in Table 1. Two parent materials were used, i.e. Domex 350 XP and Weldox 900.

Table 1 Experiment details of Lopez Martinez and Korsgren's investigation [1]

Weld method	MMA	GMA		
Filler metal	OK 48.00	PZ6130	PZ6111	OK 12.51
Gas	----	Mison 25, 15l/min	Fogon 20, 14l/min	Mison 25, 8l/min
Welding position	1G	1G	1G	1G
Throat thickness	5mm Nominal	5mm Nominal	5.5mm Measured	3-4mm Nominal
Electrode Size (mm)	4	1.6	1.6	1.0
Current (A)	185	185	257	140
Voltage (V)	24	23	25	20
Heat input (kJ/mm)	2.0	1.6	1.3	0.6
Interpass Temperature (℃)	25, 110, 125, 130	25, 125, 135, 80	20, 20, 20, 20	20, 20, 20, 20
Investigation points	712	720	5824	2896
Number of spots with defects (Cold laps)	38	83	112	475
Percentage	5.3	12	1.9	35

Two testing methods were involved in the investigation: one was fatigue testing and the other was the separate test.

In the fatigue test, the fracture surfaces were investigated. A type of microdefect was identified at the weld toe as the fatigue initial spot in almost 70% of the examined fracture surfaces. These so-called cold laps are parallel to and at the same level as the original parent plate surface. Cold laps appeared as planar defects at the weld toe and differed in shape. The defects can be very different in depth (transverse to weld longitudinal direction) and length (in weld longitudinal direction). In the study [1], two cases were identified regarding cold laps: one is the cold laps created by shrinkage crack in the welding process and another is the cold laps without any influence from shrinkage crack in the welding process; see Figure 4. For the detected cold laps, two dimensions were defined as depth and length, as mentioned above. The results showed that the cold lap can vary between 0.1 mm and 3.5 mm in length and 0.05 mm and 0.8 mm in depth[1] – see Table 2.

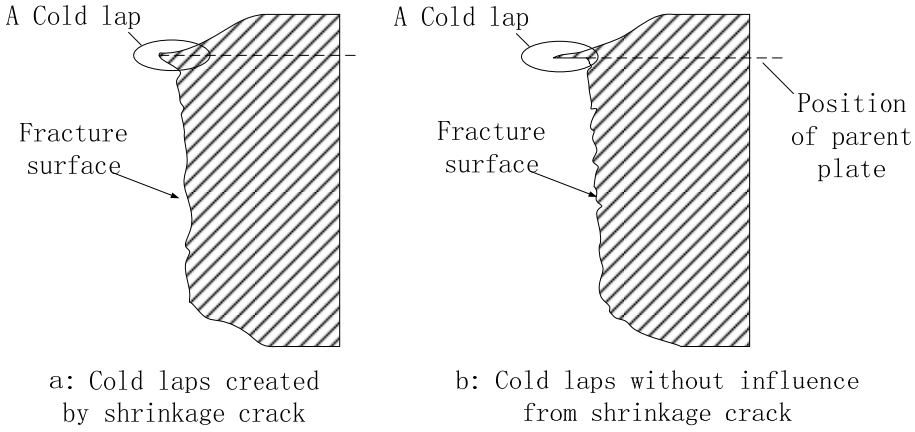

Figure 4 Two cases of cold laps identified in Lopez Martinez and Korsgren's investigation: a) Cold laps created by shrinkage crack; and b) Cold laps without influence from shrinkage crack. (Adapted from [1])

Table 2 Dimensions of the cold laps found in Lopez Martinez and Korsgren's study [1].

Dimension sketch of a cold lap (a: dimension in longitudinal direction; b: dimension in depth direction/transverse direction)	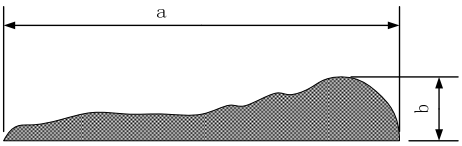		
Sample number	**a (mm)**	**b (mm)**	**Remarks**
11	0.8	0.15	
13	1.0	0.5	
14	3.5	0.5	No defects. Shape of 'early' crack
16	1.0	0.5	
18	1.5	0.4	
21	2.0	0.8	
22	0.3	0.3	Two cold laps were found for sample 22
22	1.5	0.4	Two cold laps were found for sample 22
33	0.25	0.125	
34	N.A.	<0.05	No defect? Possibly a long lack of fusion with depth <0.05 mm
67	<0.1	<0.1	

In the separate test, the weld was cut and the cross sections were milled, polished (down to 3 μm), and etched (3% Nital). New cross sections were prepared using the same procedure 2 mm away from the former cross section. A microscope was used to examine the defects on the cross section at two magnifications (50 x and 200 x magnification). Th depth (d) and orientation (ψ) of defects were evaluated, as shown in Figure 5 [1].

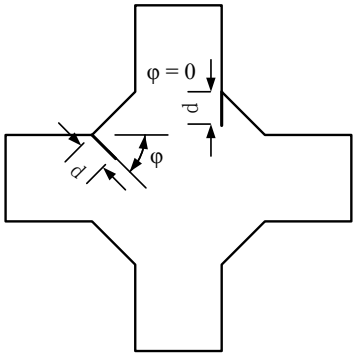

Figure 5 Depth (d) and orientation (ψ) of the tested sample (Adapted from [1])

The number of cross sections (investigation points) for different welding specimens is listed in Table 3. In Lopez Martinez and Korsgren's paper [1], it is stated that the defects found in separate tests can be regarded as cold laps based on the discovery in the fatigue test. However, the cold laps found in the fatigue test were stated to be mainly parallel to the parent metal surface. The defects of 90^{o} orientation can be an exception of cold laps, or they may be due the 'shrinkage crack' [1]. Also, their formation could be different. Therefore, the defects with 90^{o} are not considered in this thesis. To illustrate the frequency of defects for different welding methods and materials, the percentage of investigated points with defects was evaluated. The mean value of the defect length of the cross section was record and calculated. The results are shown in Table 3.

Table 3 Separate test result for defects on the prepared cross sections (Adapted from [1])

Weld method	MMA	GMA		
Filler metal	OK 48.00	PZ6130	PZ6111	OK 12.51
Investigation points	712	720	5824	2896
Number of spots with defects (cold laps)	38	83	112	475
Percentage (%)	5,3	12	1,9	35
Mean value in d (mm)	0.270	0.250	0.047	0.130
STEDV	0.300	0.250	0.050	0.150

From the results shown in Table 3, only a small difference between OK 48.00 (basic electrode) and PZ6130 (basic flux cored wire) in terms of cold lap mean depth was found. The PZ6111 (rutile flux cored wire) gave the smallest defects in depth. The OK 12.51 (solid wire) gave the highest frequency of cold laps. Hence, the type of electrode has the most significant influence on cold laps. Basic filler materials tend to give a deeper cold lap. Solid wires tend to give a higher frequency of cold laps. In comparison, as shown in Table 1, the effects of current, voltage, and heat input on cold laps are weak.

According to Samuelsson [2], cold laps are a local lack of fusion. This definition of lack of fusion makes it easier to understand cold lap comprehensively. Furthermore, the importance of the

lack of fusion definition is to imply cold lap formation as the conventional lack of fusion, e.g. lack of energy/heat, improper preweld cleaning, and incorrect welding techniques/operation, etc [11].

3.2 Detection of cold laps

As mentioned above, cold laps are very small in size (0.1 mm-3.5 mm in length and 0.05 mm-0.8 mm in depth). It is very hard to detect cold laps by any NDT method. The conventional method for detecting cold laps is cutting, polishing and investigating the cross section by microscopy.

However, this method cannot give information about the length of the cold laps along the weld bead. Also, it is hard to get an overview of the number of cold laps in the weld. Therefore, a new destructive method was developed by Holst et al. [5] which can successfully detect cold laps.

To prepare the specimen, the first step is to grind a gap on the opposite side of the weld. The location of the gap is the plate thickness plus half the throat thickness from the edge of the base metal, and the depth is half the plate thickness. The position and depth can be seen schematically in Figure 6 [5]. If the gap is too deep or too far from the edge, the bending will not occur at the right place and nothing can be gathered [5].

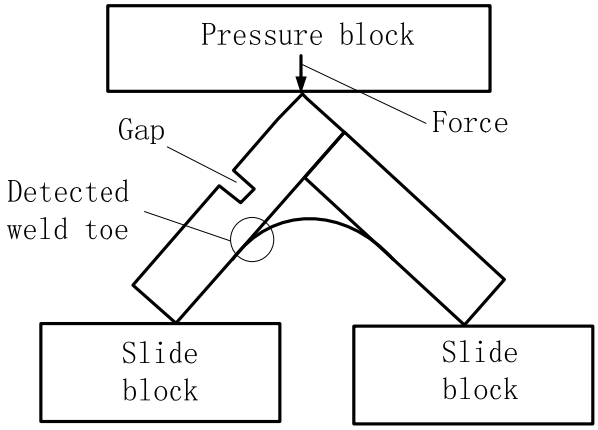

Figure 6 The correct position and depth of the gap (Adapted from [5]). The location of the gap is the plate thickness plus half the throat thickness from the edge of the base metal and the depth is half the plate thickness.

To bend the specimen, the specimen needs to be placed on plates which can slide apart as the press goes down until the weld is torn completely. A spacer can be placed on the top to spread the force over the specimen. The force needed varies with the depth of the gap, length of the specimen, thickness of plate, design, throat thickness, and geometry.

In the first stage, the weld tears up at the weld toe. In the next stage, the crack propagates through the material and finally the specimen splits into two pieces, as shown in Figure 7. It is important to protect the edge of the fractured surface.

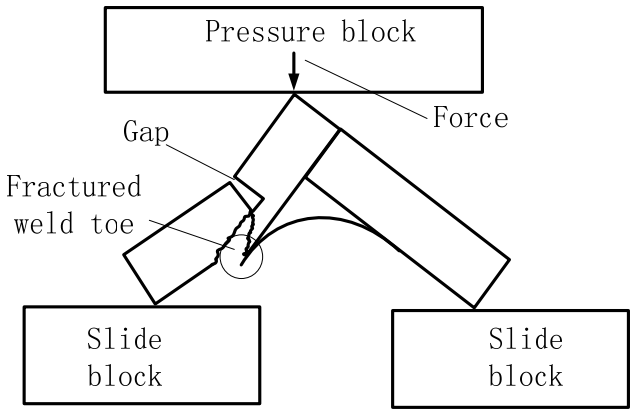

Figure 7 Fractured weld toe. (Adapted from [5]) The detected weld toe is torn up with the pressure and tow slide blocks. Finally, the specimen splits into two pieces.

To examine the specimen, a stereo microscope with magnification of 4-6 times is suggested. For a more exact defect size determination, a camera connected to a computer can be used. Cold laps and spatters were identified on the fracture surface of the weld toe in the work of Holst et al. [5].

Therefore, using the method above, it is possible to perform a destructive test of a specimen to indicate cold laps, spatters, lack of fusion and pores for solid electrode MAG-welds. Both the length and the depth of the cold laps can be determined.

3.3 Previous classification of cold laps

Cold laps were characterized and categorized by Farajian-Sohi and Järvstråt [12]. In the experiment, tandem GMAW welding was used. Structural steel (EN 10 025-S275JR) plates were used as the base metal and were plasma-cut into smaller coupons with the dimensions of 12*50*300 mm. Welding was performed on the plate (bead-on-plate). As-milled steel plates and weld position PA were chosen for the experiment. Thirty-eight welded specimens with different welding parameters were produced. When selecting the welding parameters, spray mode was ensured, even for different arc lengths engaged. Also, the ratio of wire feed speed (WFS) and travel speed (TS) was kept fixed to keep the same deposition rate in which different weld profiles were produced. The influence of electrode stick-out can be studied by varying contact tube to work piece distance (CTWD). The influence of the welding torch angle (forward and backward) was also studied. The WFS of the leading wire was kept always equal to that of the trailing wire. Two combinations of electrodes, i.e. solid-solid and solid-cored wire, were used in the experiment.

A developed rapid destructive method was used to detect cold laps in which the specimens were hit by a pendulum tip in an impact test machine. After breaking the specimens, the fracture surface of the broken parts was studied using light optical and scanning electron microscope. The tests with different loading speeds showed that a faster loading speed and a lower temperature could give a better picture of the imperfections. In order to fracture the parts in a brittle manner, the specimens were first cooled down in a container filled with liquid nitrogen for 10 minutes before the impact test. The test coupons were prepared with the dimension 11*12*50 mm. The pendulum hits the specimens from behind and breaks them by propagating a crack starting at the weld toes. In Figure 8, the specimen preparation and impact testing are described schematically [12].

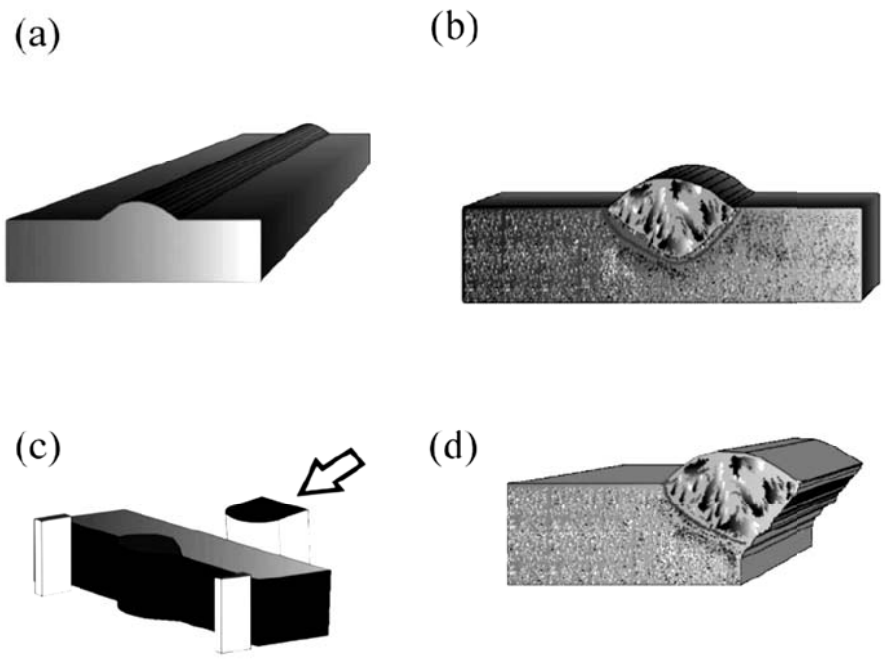

Figure 8 Schematical description of the test: a) Bead on plate weld specimen. b) Slicing the specimen into sub-specimens. c) Hitting with a pendulum. d) Light or electron microscopy of the fracture surface [12] (Originally published in Steel Research International, 77 (2006), No. 12, pages 889-895. With permission.)

By studying the fracture surfaces, the initial imperfections which exist between the weld toe and base material could be observed. The fracture surfaces from this impact test and the previous fatigue tests were compared. Cold laps can be observed clearly in both methods. Using these experiments, Farajian-Sohi and Järvstråt [12] observed two types of cold laps, known as 'overlap' and 'spatter'.

In Figure 9, overlap was observed as solidified overflow of the weld pool on the base metal. A sharp contrast can be observed between the base material fracture surface and the sub-fracture surface of the overlaps (see Figure 9a). Three overlaps were shown at the weld toe in Figure 9. The details of the encircled imperfection in Figure 9a are shown in Figure 9b at a higher magnification. A semi-elliptical crack-like imperfection was observed which is 1.5 mm long and 0.45 mm deep. The observation of the imperfection showed no metallic binding with the base material. The sub-surface of the cold laps appeared porous. In the large pores, some solid inclusions can be observed [12].

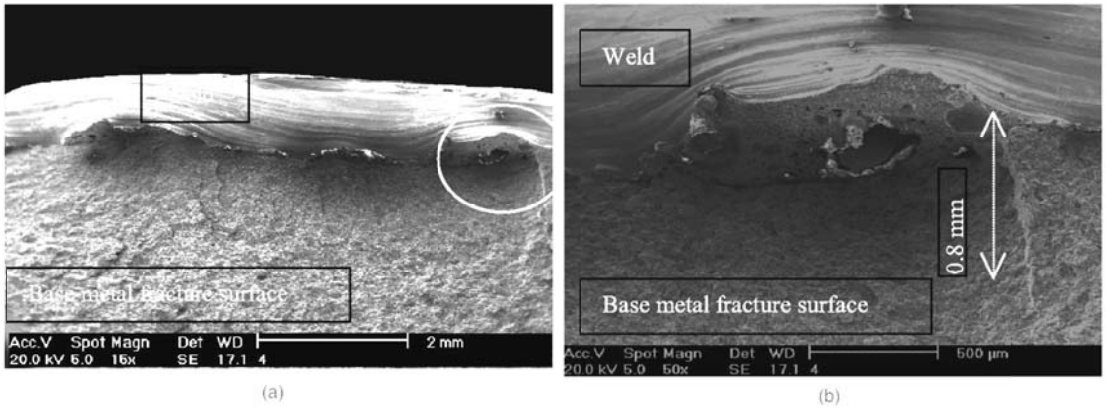

Figure 9 Overlap found in [12]. a) Scanning electron microscopy of the fracture surface of the welded specimen containing overlap-type cold laps. b) Magnification of the cold laps circled in a) [12] (Originally published in Steel Research International, 77 (2006), No. 12, pages 889-895. With permission.)

To study the elements present on the observed cold lap surface, energy dispersive spectroscopy (EDS) investigation using the scanning electron microscope was performed at the point where solid inclusions were dominant, as shown in Figure 10 . The results from the EDS analysis showed that silicon and manganese were present on the surface in addition to iron, oxygen and carbon, as shown in Table 4. This suggests that the silicon and manganese inclusions were trapped between the weld and the base metal, forming the non-metallic bonding layer during the welding and solidification process.

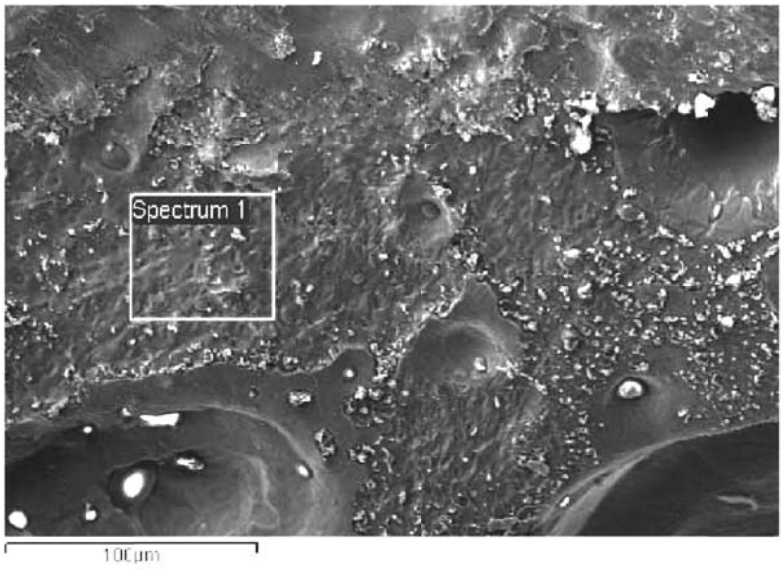

Figure 10 Surface of a cold lap investigated using EDS [12] (Originally published in Steel Research International, 77 (2006), No. 12, pages 889-895. With permission.)

Table 4 Chemical composition obtained by EDS investigation of one cold lap surface, as shown in Figure 10. (Modified from [12])

Element	Weight (%)	Atomic (%)
C	2.07	7.31
O	9.11	24.15
Si	0.91	1.37
Mn	1.50	1.16
Fe	85.75	65.13

Another type of cold lap found by Farajian-Sohi and Järvstråt [12] is named 'spatter'. The length of a single spatter is much shorter than that of the overlap-type cold laps, and in general the aspect ratio (a/c a: crack depth, 2c: crack length) of spatter-like cold laps is larger than that of overlap-like cold laps. In Figure 11, a single spatter trapped within the weld metal at the weld toe is shown. The observed spatter has a diameter of around 200 µm and was believed to be covered by the weld weaves. Some oxides were also found surrounding the spatter, which is the same material as the inclusions in the pores on the overlap surface. A cluster of spatter was also observed at the edge of the fracture surface, as shown in Figure 12. Between the sticking spatters, oxides and pores were stated to be found. The length of this spatter cluster is 1.8 mm and its depth is 0.6 mm.

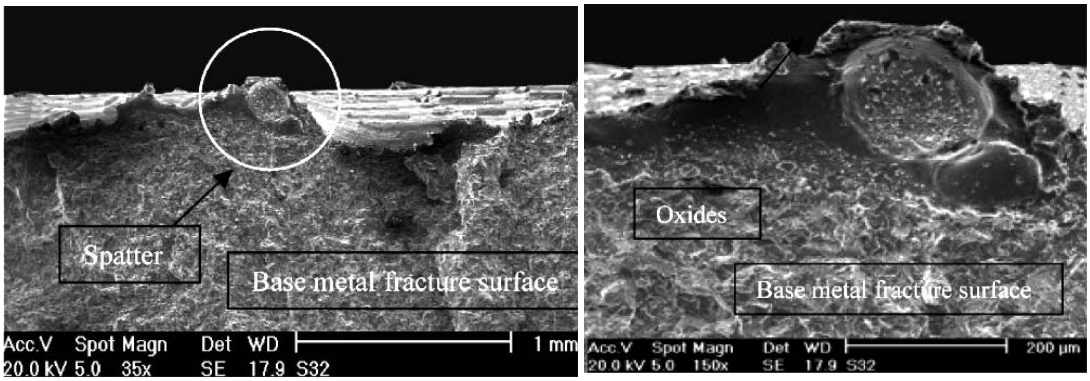

Figure 11 Spatter found in [12]. a) Single spatter on the top of the fracture surface. b) Magnified picture of the spatter in the left image. [12] (Originally published in Steel Research International, 77 (2006), No. 12, pages 889-895. With permission.)

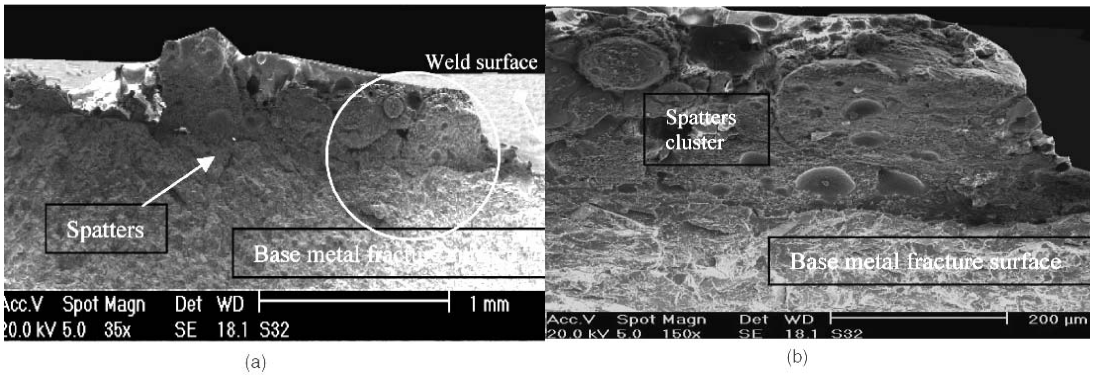

Figure 12 a) Cluster of spatter on the top of the fracture surface. b) Magnified picture of the part circled in a) [12] (Originally published in Steel Research International, 77 (2006), No. 12, pages 889-895. With permission.)

In the discussion of the paper [9], the authors stated that several force fields in the welding process, e.g. arc pressure, electromagnetic fields and the force from the shielding gas flow, result in the fluctuation of the weld pool. The fluctuations are the source of the ripple of the weld. If the force fields which control the fluctuations of the weld pool were disturbed, larger ripples would be produced. When the larger ripples with higher kinetic energy than normal ripples reach the weld toe, they overlap on the base metal and form the overlap type of cold lap together with the cold base metal surface. The solid inclusions containing silicon and manganese were regarded to be trapped particles which are produced during welding. The silicon and manganese inclusions were assumed to be products of deoxidization of the electrodes and cleaners for base metal surfaces containing oxides/mill scale. It was stated in [12] that gases can be released while the inclusion is solidifying.

3.4 Influence factors for cold laps

For a deeper understanding of cold laps, it is important to understand the influence factors which are supposed to be able to significantly control the occurrence and dimensions of cold laps.

Robotic Rapid Arc GMAW (high speed welding) with solid wire was used by Hedegård [13] to produce welding specimens. Fillet welds were produced in the experiment. A destructive method (cross sections of the weld) was used to detect and evaluate cold laps.

Table 5 Seven varied important welding parameters in experiment. (Adapted from [13])

Examined welding parameter	Value of two levels
Electrode stick-out	22/29 (mm)
Heat input	0.8/1.1 (kJ/mm)
Welding gun angles	A/B (not specified in paper)
Welding gun position	e.g. bad position: 1/0 (mm) off
Welding position	1F/2F
Surface quality of the plate	Blasted/as delivered
Weld size (throat size)	4/6 (mm) throat size

In the experiment, multi-factorial tests were performed and eight test series were welded, consisting of three specimens each. Seven important welding parameters were varied in a standardised and reduced two-level multi-factorial test. The welding parameters examined are shown below.

In total, twenty-five independent cuts were made for each series. By evaluating the cross sections, three significant parameters were revealed for cold lap occurrence, i.e. welding position, surface condition, and welding gun position [13].

The most important parameters for GMAW, as considered by Farajian-Sohi and Järvstråt [14] in their experiment, are listed in Table 6.

Table 6 Nominal weld parameters. (Controlled parameters are denoted by *, those held fixed are denoted by °, and those fully determined by controlled parameters are denoted by †.) (Adapted from [14])

Welding parameter	**Base material**	**Filler materials and Shielding gas**
Total wire feed speed* (21 m/s)	Alloy° (Steel, EN 10 025-S275JR)	Wire type* (solid: OK Autrod 12.51, metal cored: OK Tubrod 14.12)
Weld torch angle* (0, vertical)	Plate thickness° (12 mm)	Wire diameter° (1.2 mm, leading and trailing)
Arc length* (4 mm)	Surface quality° (As rolled)	Distance between the two contact tubes° (20 mm)
Contact tube to work distance (16 mm)*	geometry° (50×300 mm, bead-on-plate)	Gas type*: 92% Ar and 8% Co2
Electrode stick-out†	Welding position° (Horizontal, PA)	Gas flow rate° (28 l/min)
Current†		
Voltage†		
Welding speed†		

A fractional factorial two level model with one replication was chosen to design the experiment using the software MODDE. Six variables of the welding parameters for tandem GMAW with two levels were involved in experimental design, as shown in Table 7 [14].

A total number of 38 weld specimens with different and controlled welding parameters were produced according to the work sheet, as shown in Table 8 [14]. Strangely, the two level of CTWD used are 13 mm and 15 mm instead of the levels shown in Table 7.

Table 7 Welding variables and their ranges in the paper. (Adapted from [14])

Tandem arc welding parameters	Notation	Range
Wire Feed Speed	WFS	18, 21, 24 (m/s)*
Arc Length (Leading)	Larc	2,4,6 (mm)
Contact Tube to Work Distance(Leading)	CTWD	15, 16, 17 (mm)*
Torch Angle	TA	-10(Pull), 0, 10(Push) degrees
Wire combinations	WireC	Solid-solid: 0 Solid-cored: 1
Weld Speed (Set to WFS/15)	WS	1.2, 1.4, 1.6 (m/s)*

*The three values refer to the low, mid and high level of the variables. With the middle value the repetitions were given.

Table 8 Work sheet of welding parameters. (Adapted from [14])

No.	WFS (m/min)	WS (m/min)	Larc (mm)	CTWD (mm)	TA	Wire type	Voltage Leading (V)
1.20	18	1.2	2	13	-10	Cored	27.5
2.21	24	1.6	2	13	-10	Solid	29.0
3.22	18	1.3	6	13	-10	Solid	29.8
4.23	24	1.6	6	13	-10	Cored	34.8
5.24	18	1.2	2	15	-10	Solid	26.0
6.25	24	1.6	2	15	-10	Cored	29.5
7.26	18	1.2	6	15	-10	Cored	32.0
8.27	24	1.6	6	15	-10	Solid	34.8
9.28	18	1.2	2	13	10	Solid	26.0
10.29	24	1.6	2	13	10	Cored	29.5
11.30	18	1.2	6	13	10	Cored	31.5
12.31	24	1.6	6	13	10	Solid	34.8
13,32	18	1.2	2	15	10	Cored	27.5
14.33	24	1.6	2	15	10	Solid	29.5
15.34	18	1.2	6	15	10	Solid	29.5
16.35	24	1.6	6	15	10	Cored	34.8
17	21	1.4	4	14	0	Cored	31.0
18	21	1.4	4	14	0	Cored	31.0
19	21	1.4	4	14	0	Cored	31.0
36	21	1.4	4	14	0	Solid	29.6
37	21	1.4	4	14	0	Solid	29.6
38	21	1.4	4	14	0	Solid	29.6

To evaluate the specimens, both the conventional cross-section method and the developed impacted destructive method (as mentioned in the above chapter) were engaged. Light optical and scanning electron microscope was used for the investigations. Two types of cold lap were observed in this study [14], i.e. overlap and spatters, and Mn and Si inclusion was also found on the surface of the flaw [14].

The depth of the two types of cold laps for all the fractured specimens was measured. The maximum defect depth was registered over a distance of about 11 cm for each set of weld parameters. In Figure 13, histograms showing defect depth ranges measured from all the detected toe flaws are given.

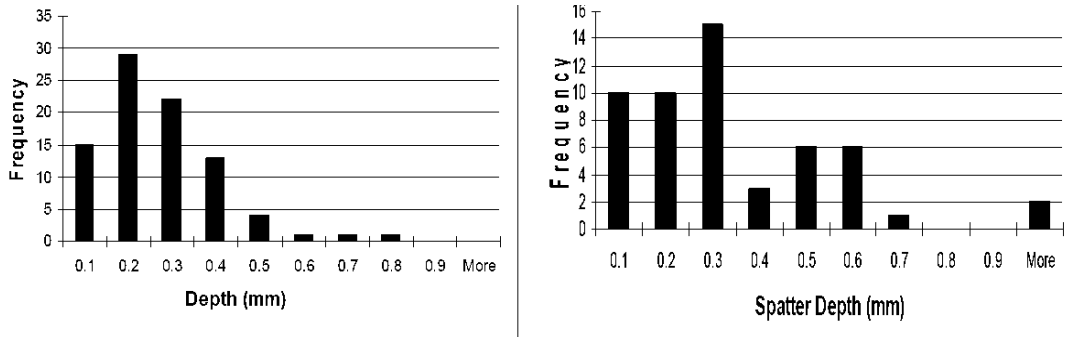

Figure 13 Histograms of the depth of a) overlap and b) spatter [14] (Reprinted with permission of ASM International. All rights reserved. www.asminternational.org)

The histograms show that the overlap depth has a normal distribution with an average value of 0.25 mm and that spatters are randomly distributed with an average depth of 0.34 mm.

The effect of the different parameters was statistically evaluated using the software MODDE. For overlaps, Farajian-Sohi and Järvstråt [14] stated that the factors with the most pronounced effect on the overlap depth were the total wire feed speed (WFS) and the torch angle (TA), as shown in Figure 14. The contact tube to work piece distance (CTWD) had a minor effect but still statistically significant.

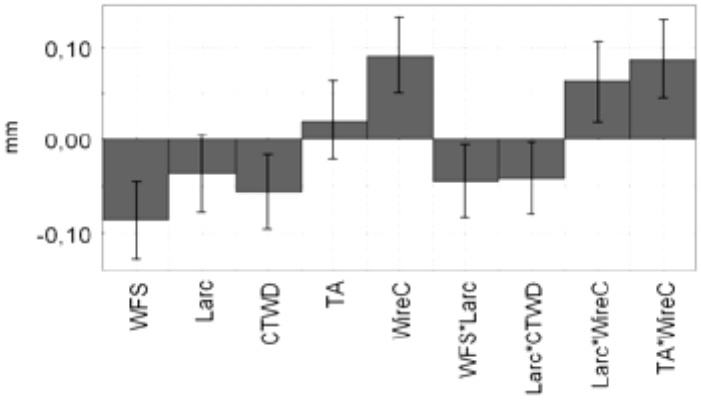

Figure 14 Scaled and cantered coefficient plot of parameters affecting maximum overlap depth in 110 mm of welds. [14] (Reprinted with permission of ASM International. All rights reserved. www.asminternational.org)

The statistically derived empirical models were also given, as shown in equation 1 and 2.

For solid-solid wire:

$$Max\ overlap\ depth = 4 - (0.22 + 0.006 \cdot Larc - 0.01 \cdot CTWD) \cdot WFS - (0.06 + 0.001 \cdot Larc + 0.004 \cdot CTWD) \cdot TA + 0.5 \cdot Larc - 0.21CTWD - 0.03 \cdot Larc \cdot CTWD \quad \text{Eq.(1)}$$

For solid-cored wire:

$$Max\ overlap\ depth = 3.45 - (0.23 + 0.006 \cdot Larc - 0.01 \cdot CTWD) \cdot WFS - (0.04 + 0.001 \cdot Larc + 0.004 \cdot CTWD) \cdot TA + 0.56 \cdot Larc - 0.23CTWD - 0.03 \cdot Larc \cdot CTWD \quad \text{Eq.(2)}$$

For the spatters, using the same method, the authors stated that the total wire feed speed (WFS) and the torch angle (TA) were dominating factors, as shown in Figure 15 .

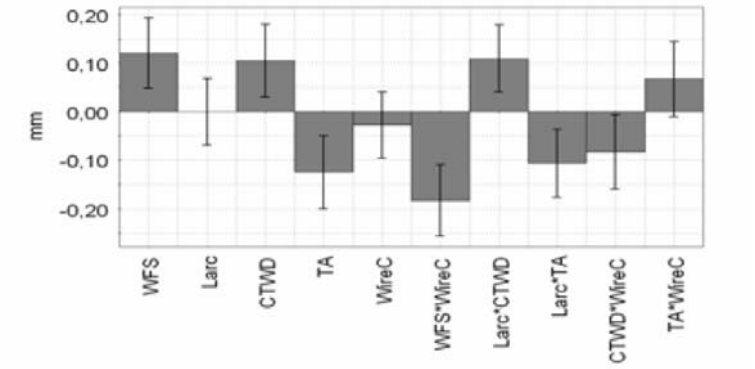

Figure 15 Scaled and centred coefficient plot of parameters affecting maximum spatter depth in 110 mm of welds. [14] (Reprinted with permission of ASM International. All rights reserved. www.asminternational.org)

Regarding the overlap, if the equations (Eq.1 and Eq.2) are reliable and able to be simplified, neglecting the interacted items, the new equations can be written as:

For solid-solid wire:

$$Max\ overlap\ depth = 4 - 0.22 \cdot WFS - 0.06 \cdot TA + 0.5 \cdot Larc - 0.21 \cdot CTWD \quad \text{Eq.(3)}$$

For solid-cored wire:

$$Max\ overlap\ depth = 3.45 - 0.23 \cdot WFS - 0.04 \cdot TA + 0.56 \cdot Larc - 0.23 \cdot CTWD \quad \text{Eq.(4)}$$

Considering the change range of the value for each parameter, the maximum effect of each parameter can be calculated, as follows:

For solid-solid wire:

$$Max\ effect\ of\ WFS = \pm(-0.22) \cdot WFS = \pm(-0.22) \cdot (24 - 18) = \pm(-1.32) \quad \text{Eq.(5)}$$

$$Max\ effect\ of\ TA = \pm(-0.06) \cdot TA = \pm(-0.06) \cdot (10 + 10) = \pm(-1.2) \quad \text{Eq.(6)}$$

$$Max\ effect\ of\ Larc = \pm 0.5 \cdot Larc = \pm 0.5 \cdot (6 - 2) = \pm 2 \quad \text{Eq.(7)}$$

$$Max\ effect\ of\ CTWD = \pm(-0.21) \cdot CTWD = \pm(-0.21) \cdot (17 - 15) = \pm(-0.42) \quad \text{Eq.(8)}$$

For solid-cored wire:

$$Max\ effect\ of\ WFS = \pm(-0.23) \cdot WFS = \pm(-0.23) \cdot (24 - 18) = \pm(-1.38) \quad \text{Eq.(9)}$$

$$Max\ effect\ of\ TA = \pm(-0.06) \cdot TA = \pm(-0.04) \cdot (10 + 10) = \pm(-0.8) \quad \text{Eq.(10)}$$

$$Max\ effect\ of\ Larc = \pm 0.5 \cdot Larc = \pm 0.56 \cdot (6 - 2) = \pm 2.24 \quad \text{Eq.(11)}$$

$$Max\ effect\ of\ CTWD = \pm(-0.23) \cdot CTWD = \pm(-0.23) \cdot (17 - 15) = \pm(-0.46) \quad \text{Eq.(12)}$$

From Eq.5 to Eq.12, some agreement can be seen with the authors on the effect of WFS, TA and CTWD. However, it is obvious that the arc length has the greatest effect on the depth of overlap cold lap for both solid-solid wire and solid-cored wire. Physically, the arc length means the voltage in the weld process, from which the conclusion can be drawn that welding voltage has the most significant effect on overlap depth. For the spatters, the same arguments can also be raised.

Moreover, the authors [14] also concluded that switching from a solid-solid wire combination to a solid-cored wire combination resulted in deeper overlap, as shown in Figure 16 and Figure 17. However, from the previous work of Lopez Martinez et al. [1] and Hedegård et al. [13], a contradictory conclusion was drawn that the solid wire gave deeper cold laps compared with cored wire in a single wire or Rapid Arc welding process (see chapters 2.1 and 2.5). One explanation for the contradictory results was given by Farajian-Sohi and Järvstråt [14]. The authors stated that the experiments were performed on as-rolled metal sheets and the surface quality was not optimal. Therefore, the surface impurities had a dominant effect in producing the contradictory results with the previous work. However, if it is true that the surface condition has a dominant effect, all the results could be questionable.

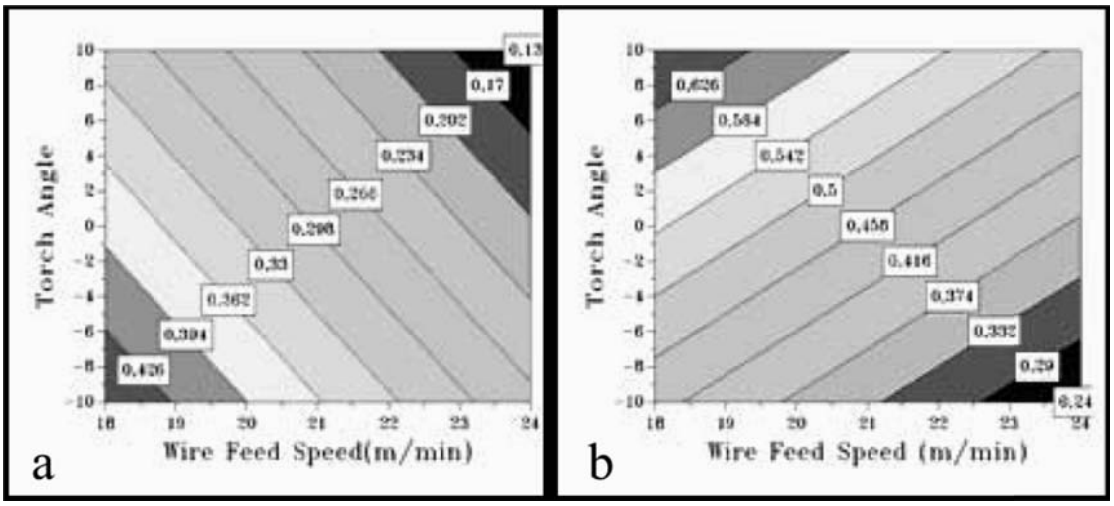

Figure 16 Statistical model representing a) Depth of overlap for solid-solid wire. b) Depth of overlap for solid-cored wire. [14] (Reprinted with permission of ASM International. All rights reserved. www.asminternational.org)

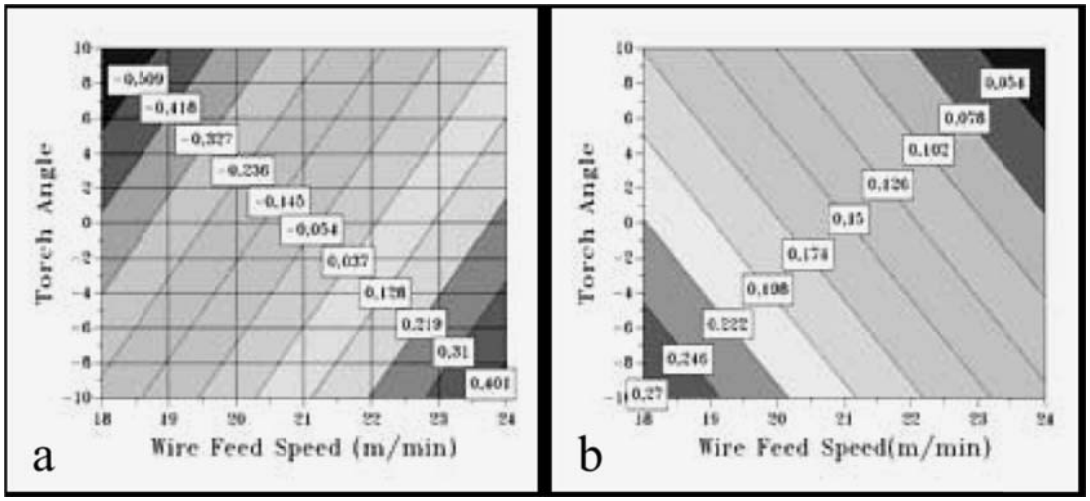

Figure 17 Statistical model representing a) Depth of spatter for solid-solid wire. b) Depth of spatter for solid cored wire. [14] (Reprinted with permission of ASM International. All rights reserved. www.asminternational.org)

Furthermore, it is well known that the selection of independent factors is statistically important for the experimental design. However, in the study [14], the authors selected arc length and contact tip work distance (CTWD) as the factors in their fractional factorial experimental design. As discussed in chapter 2, the arc length and CTWD are not independent factor with the fixed stick-out. Therefore, this independence could also give poor statistical significance in the experimental design of the paper.

Lopez Martinez et al. [15] produced welds by MAG using blasted Weldox700 as the base material. Before the fatigue test, TIG-dressing was performed on the weld toes. The failure specimen in the fatigue test was prepared so that the fracture surfaces could be analysed using an optical microscope and a scanning electron microscope to identify the initial points of fatigue. By this observation, cold laps were found in the specimens after TIG dressing but at a lower depth. The results showed that TIG dressing cannot eliminate the cold laps from the weld toe, but can only reduce the depth of the cold laps.

4 Oxides in GMAW process

Welding can be regarded as a metallurgy process with quick melting, cooling and solidification. From this rapid process, a sound weld is produced with high strength and toughness compared with the parent material. The alloy elements in the weld metal are the key to ensuring the required mechanical properties. For the GMAW welding process, both droplet and weld pool will experience an extremely high temperature, and oxidization is inevitable. This oxidisation will consume a certain amount of the beneficial alloy elements. For different parent materials, the beneficial elements can be different. On the other hand, the alloy elements are important for the weldability in terms of being free from welding flaws, e.g. proper viscosity of the molten metal, a lighter oxide which can easily flow up to the weld pool surface, etc. For these purposes, there are a large number of alloy elements, e.g. C, Si, Mn, Cr, Ni, V, Ti, Co, Mg, N, Mo, Zr, Nb and Al, etc [8, 9, 11]. However, only the behaviour of manganese and silicon is focused on in this study, since Mn-Si oxides were found to be the major oxides in cold laps.

Manganese is a greyish-white metallic element with an atomic weight of 54.9 and a melting point of 1245^{o}C. A certain quantity of manganese can commonly be found in most steels, as it is a helpful additive in iron alloys. Manganese has a stronger affinity to oxygen, sulphur and carbon than iron. When added to molten iron, manganese reacts with oxygen to form manganese oxide (MnO). Hence, manganese is a deoxidizer for iron, but it is still less important than aluminium and silicon. In the melt, Manganese can also react preferentially with sulphur to form manganese sulphur (MnS). Therefore, the MnS inclusion is common in hot rolled steel as a thin layer inclusion. Manganese is commonly found as an alloying addition in all types of carbon and low-alloy-steel base metals and filler metals for welding. The purpose of manganese can generally be summarized as being threefold [16]:

- Combines with oxygen in the molten steel as a deoxidizer;
- Ties up any sulphur that may be present to avoid hot cracking;
- Promotes greater strength by increasing the hardenability of the steel (toughness is usually improved as a bonus effect)

Silicon has an atomic weight of 28 and a melting point of 1427^{o}C. Silicon is used mainly in steels as a deoxidizing agent. In steelmaking, the amount of silicon to be added is slightly in excess of the quantity needed to combine with the oxygen. Silicon and oxygen react vigorously to liberate a large amount of heat, and silicon dioxide (SiO_2) is formed. The silicon dioxide can either escape to the molten metal surface or form inclusions in the solidified steel. With the presence of manganese in the molten steel, the silicon dioxide inclusions will often occur as complex iron-manganese silicate compounds. If manganese and silicon are added together and act synergistically, the manganese and silicon can achieve a non-metallic composition that will remain liquid at the freezing temperature of the steel [16]. The silicon can also be used as a ferrite strengthener, and it is stronger in this respect than most other commonly used alloying elements. Also, silicon is a strong hardenability promoter. Therefore, heat-treatable alloy steels have a high proportion of silicon. Finally, silicon can promote the fluidity of the molten steel. It is sometimes useful in pouring castings and in certain fusion-welding processes.

In the molten steel, the deoxidation of silicon and manganese can give complex products, even for the equilibrium condition. According to Turkdogan [17], the products will be determined by all three factors, i.e. the content of silicon and manganese, the content ratio between silicon and manganese, and the temperature, as shown in Figure 18.

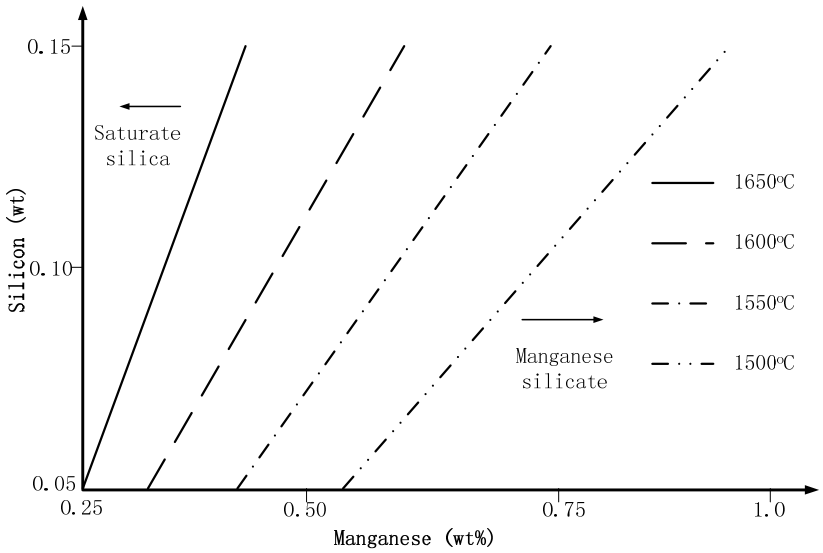

Figure 18 Products of oxidation of silicon and manganese in equilibrium molten steel. (Adapted from [17])

However, the oxidation products of silicon and manganese could be more complex because the welding process generally features a rapid cooling process, making it hard to achieve equilibrium conditions in the molten material. Also, it is hard to measure the temperature in the welding process. Grong and Christensen [18] performed an experiment in an enclosed chamber. Different shielding gases were used in the experiment. Basically, two types of specimens were prepared: one is a chilled weld metal and the other one is a multi-layer weldment. The electrode tip after welding was also analysed.

For the chilled weld metal samples, the weld was made on a water-cooling copper wheel which was covered by a Teflon scraper to ease the weld metal separation. The chilled metal was collected in the form of intermittent strips (1 to 2 mm wide, thickness 0.05 to 0.1 mm, length 20 to 150 mm).

For the multi-layer weld metal, the welding trials were performed on mild steel coupons (135 mm x 95 mm x 15 mm). Six layers were deposited for each sample. The welding speed was 3 mm/s. Only the top beads were investigated with respect to C, O, Si and Mn content.

A filler wire of 0.8 mm diameter was used. The rate of wire feed (about 125 mm/s) was adjusted to the operational conditions (90 to 100A and 24 to 26V, respectively). The chemical composition of the filler wire is shown in Table 1.

Table 9 Chemical composition of the filler wire. (Adapted from [18])

Elements	C	O	Si	Mn
Content (wt %)	0.097	0.020	0.83	1.52

Both electron probe analysis and chemical analysis were performed for the samples. A comparison between the results of the chilled weld metal and the multi-layer weld metal revealed that the oxidizing reaction of carbon does not normally take place in the weld pool, but occurs either at the electrode tip or in the arc plasma, or maybe both. Grong and Christensen [18] also discussed that it is reasonable to assume that the oxidation mainly occurs on the electrode tip, rather than in the arc plasma. The large metal/atmosphere interface is the main reason for CO nucleation during droplet formation. Two parts of the droplet were distinguished in the discussion of carbon oxidation. One is the hot layer, which refers to the part facing the arc. This part is most likely the location of carbon oxidation. The other part is the part on the side of the electrode wire (the lower temperature part compared with the part facing the arc) in which Si and Mn are expected to protect carbon from oxidation. When reaching the critical CO gas pressure, the carbon reaction is blocked. Thus, silicon and manganese will take over and control the oxygen level in the metal. One reason for the lack of carbon oxidation in the arc plasma is an inadequate supply of oxygen due to Mn and Fe vapour arising from metal superheating. In the hot part of the weld pool (the part simultaneously beneath and following the arc), the plasma jet blows the Mn and Fe vapour away and provides a steady supply of oxygen. However, the metal/atmosphere interface may be too small in volume compared with the droplets to limit the carbon oxidation in this stage. In the cooler part of the weld pool (the part next to the arc in the weld pool), Si and Mn are normally expected to prevent any carbon reaction.

Regarding the losses of silicon, Grong and Christensen [18] concluded that losses of silicon mainly occur in the weld pool and the amount of Si lost on the electrode tip and in the arc plasma is much smaller. Since no slag is formed on the surface of the chilled metal sample, the authors believe that the silicon must escape in the form of a gaseous product. On the other hand, evaporation losses can be excluded in this case due to a very low Si vapour pressure at the prevailing temperature. Therefore, it is reasonable to assume that SiO is formed on the tip droplet surface. The silicon losses of chilled metal with increasing oxygen potential of shielding gas are believed to be caused by the reaction:

$$SiO_2 \text{ (in slag)} + CO \text{ (g)} = SiO \text{ (g)} + CO_2 \text{ (g)}$$

When comparing the manganese content between the chilled metal samples and the multi-layer weld metal samples, Grong and Christensen [18] believed that the losses of Mn are mainly due to vaporization during extremely high temperature arc plasma (2400^{o}C).

In their conclusion, the authors summarized the results by different location in the welding process, i.e. electrode tip, arc plasma, hot part of the weld pool, and the cooling part of the weld pool. For the electrode tip, the temperature was stated to be about 1600^{o}C and carbon monoxide and manganese silicate slag were formed. Carbon was lost mainly in this stage as well. A certain amount of silicon was lost as a result of SiO formation in the fumes.

For the arc plasma, with a temperature of about 2400^{o}C, the precipitated manganese slag in the former stage re-dissolves in the metal upon heating. Further absorption of oxygen will be prevented by Fe and Mn vapours. Fumes are formed by metal vapour reacting with oxygen.

For the hot part of the weld pool, the temperature range is 2000^{o}C to 1800^{o}C. Oxygen is, to a large extent, dissolved in the weld pool at the arc root resulting from the interaction with the plasma gas. Manganese silicate slag formation takes place simultaneously, preventing the oxygen concentration from exceeding a certain limit. A separation of microslag proceeds continuously under the existing turbulent conditions. For CO_2 welding, a CO gas barrier above the metal surface, from the decomposition of CO_2, prevents the absorption of oxygen.

In the cooling part of the weld pool, the temperature is below 1800^{o}C. Silicon and manganese react further with dissolved oxygen upon cooling. The microslag separation will be highly unfavourable due to a nearly stagnant bath. For this reason, the analytical oxygen content is highly unpredictable, but is nevertheless closely linked to the silicon and manganese concentrations in the weld metal.

5 Experimental techniques

5.1 Steel and consumable materials

In the experimental work of this thesis, Domex 355 was used as the parent material and ESAB OK Autrod 12.51 was used as the welding wire.

Domex 355 is a hot rolled cold forming steel which meets steel S355 MC in EN-10149-2. It can be used in applications such as truck chassis, cranes and earthmoving machines. The chemical composition of Domex 355 is shown in Table 10 and its mechanical properties in Table 11 [19].

Table 10 Chemical composition of Domex 355 MC (Adapted from [19])

	C	Si	Mn	P	S	Al	Nb	V	Ti
Base metal: Domex 355 MC	0.10	0.03	1.50	0.025	0.010	0.015	0.09	0.20	0.15

Table 11 Mechanical properties of Domex 355 MC (Adapted from [19])

Yield strength R_{eff} (N mm^{-2}) min	Tensile strength R_m (N mm^{-2}) min-max	Elongation on failure	
		< 3 mm A_{80} % min	≥ 3 mm A_5 % min
355	430-550	19	23

ESAB OK Autrod 12.51 is a type of solid wire covered by copper which is a standard G3Si1 wire. The chemical composition is given in Table 12.

Table 12 Chemical composition of OK Autrod 12.51

OK Autrod 12.51	C	Si	Mn	P	S
Wire/strip (%)	0.14	1.00	1.60	0.025	0.025

5.2 Shielding gases

It is well known that the shielding gas can have a significant influence on the welding process. A gas mixture of argon and carbon dioxide is the most common shielding gas used in the GMAW process. For the Ar-CO_2 shielding gases, an increased CO_2 content can change the droplet transfer mode and influence spatter generation and distribution, whereas a higher amount or pure argon will decrease the arc stability of the GMAW.

In the study presented in the first appended paper, the shielding gas used was 92Ar-8CO_2. This mixed shielding gas has been mostly used for the welding of Domex 355MC base metal with OK Autrod 12.51 wire. The welding parameter procedure followed the process used in VCE.

In the second and third papers, the main interest was focused on the effect of Mn-Si oxides on cold lap formation. Therefore, an experiment was designed with two types of shielding gases: one was an oxidizing gas, i.e. CO_2 and the other was an inert gas, i.e. pure Ar.

5.3 Sealed chamber

In order to create a non-oxidizing environment, a sealed chamber was used for the welding experiments using Ar shielding gas. The chamber is a welded stainless steel structure sealed with plastic in a way that permits free movements of the robot arm which holds the welding gun inside the chamber. A gas outlet was pre-set at the top of the sealed chamber to exhaust the air from the chamber while filling-in with shielding gas through the gas supply nozzle on the bottom of the chamber. The content of the oxygen inside the chamber was measured with an oxygen analyser mounted on the robot arm at a height of 600-800 mm above the bottom of the chamber. In the pure Ar welding, the oxygen content was kept in the range of 25-50 ppm. Also, a bracket was set on the bottom of the chamber in order to improve the ground connection from the work piece back to the welding power source. The setup of the sealed chamber is shown in Figure 19.

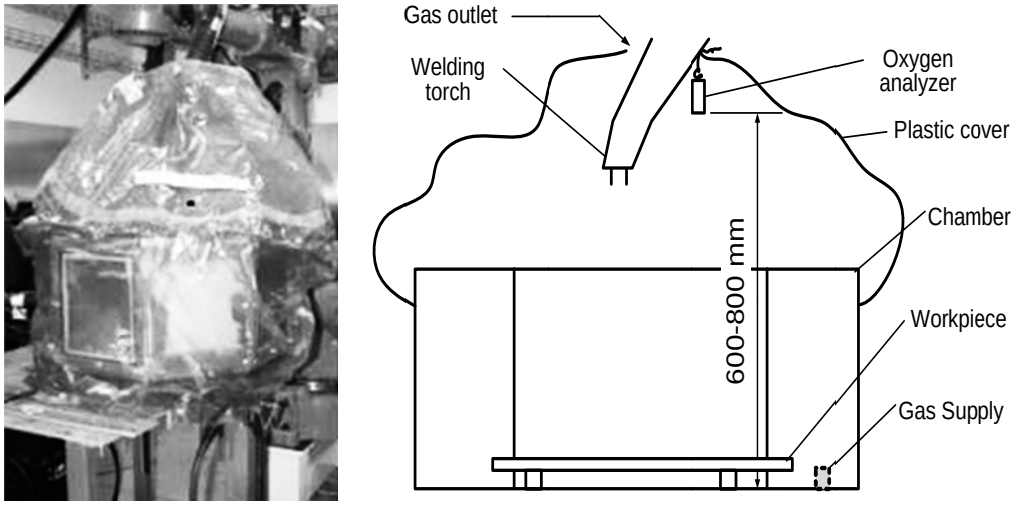

Figure 19 Schematic figure of experiment setup

5.4 SEM and EDS

A scanning electron microscope (SEM) is a materials investigation tool that can produce high resolution microstructure images with the help of a high-energy scanning electron beam. For such investigations, an electron beam is accelerated using a high voltage field in the electron gun. The high energy electrons interact with the atoms at or near the sample surface and produce signals, e.g. secondary electrons, back-scattered electrons and characteristic X-ray, as shown in Figure 20. These signals can be detected and received using an electron detector, resulting in an image of the sample surface. The secondary electron (SE) image and back-scatter electron (BSE) image are the most common image modes in SEM.

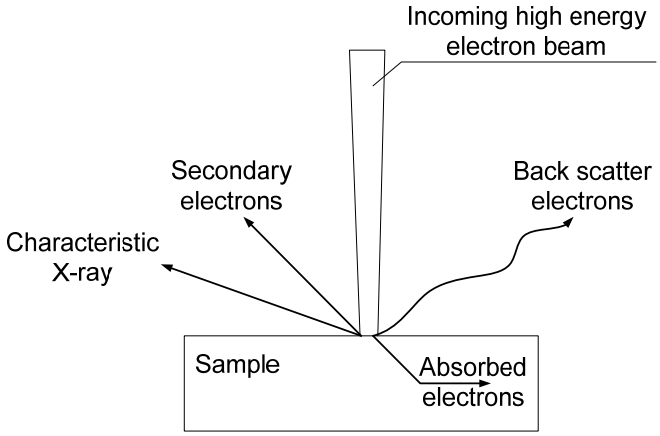

Figure 20 Signals produced in SEM

The secondary electrons have low energy due to the inelastic interaction with the atoms in the sample. Due to their characteristics, the secondary electrons come from an area very near to the sample surface. Also, the edges of the objects tend to give more secondary electrons. Therefore, SE images can usually give very high resolution surface images and can also be used to produce a three-dimensional image of the sample surface.

BSEs are beam electrons that are reflected from the sample by elastic scattering. The BSEs have high energy and can generate a large interaction volume beneath the specimen surface. Since the heavy elements can give more back-scattered electrons, BSEs are used to detect contrast between areas with different chemical compositions.

The spatial resolution of the SEM depends on the size of the electron spot and the size of the interaction volume, as shown in Figure 21. The larger electron spot and greater interaction volume give a lower resolution of the SEM. Since the interaction volume is dependent on the energy of the beam, lower beam energy is suggested when performing image analysis at the specimen surface.

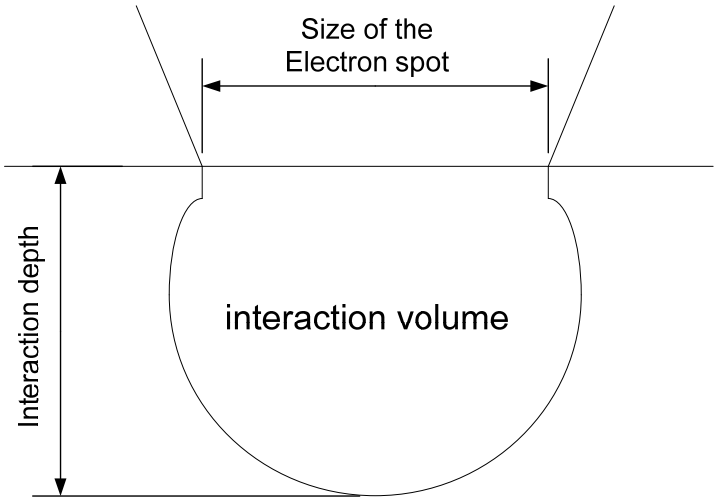

Figure 21 Electron interaction volume

The SEM used in this study was a JSM-6490LV from JOEL, which has a resolution of 3.0 nm. The low vacuum mode was used to investigate the influence of mounting material in the first

paper. The high vacuum mode was used in the work presented in the second and third papers due to the utilization of conductive mounting materials. Standard automated features were also used in the above mentioned experiments, including Auto Focus, Auto Gun (saturation, bias and alignment), and automatic contrast and brightness.

Energy-dispersive spectroscopy (EDS) is an analytical technique used for the elemental analysis or chemical characterization of a material. As mentioned above, a characteristic X-ray can be emitted when the high energy electron beam hits the sample. The number and energy of the X-rays emitted from a specimen can be measured using an energy-dispersive spectrometer. By analysing the unique X-ray, EDS allows the identification of different elements in the sample. The accuracy of the EDS spectrum can be affected by many factors. Windows in front of the detector can absorb the low-energy X-ray (i.e. EDS detectors cannot detect elements with an atomic number of less than 4, i.e. H, He, and Li). Also, many elements will have overlapping peaks (e.g. Ti Kβ and V Kα, Mn Kβ and Fe Kα). The accuracy of the spectrum can also be affected by the nature of the sample. X-rays can be generated by any atom in the sample that is sufficiently excited by the incoming beam. These X-rays are emitted in any direction, and so they may not all escape the sample. The likelihood of an X-ray escaping the specimen, and thus being detected and measured, depends on the energy of the X-ray and the amount and density of the material it has to pass through. This can result in reduced accuracy in the case of inhomogeneous and rough samples.

Two types of SEM and EDS system were used in this study. In the experiment of paper I, the SEM and EDS system is a high resolution field emission type LEO 1550 Gemini equipped with an Oxford EDS system. In the experiment of paper II and paper III, the system is a Bruker Quantax 800 system. The detector is an X-flash 4010 with a resolution of 127 eV for the Mn-K peak.

6 Summary of appended papers

Three papers have been or will be published regarding the objectives of this thesis:

- Classification of cold laps,
- Characterization of cold lap interface,
- Investigation of the influencing factors on cold lap formation.

This chapter presents a brief summary of the papers which have been reformatted for uniformity and increased readability.

6.1 Paper I

The main purpose of this paper is to classify cold laps. Secondly, the interface of the spatter/base metal is supposed to be characterized. A tandem welding experiment was performed using 92Ar-8CO2 shielding gas, Domex 355 MC base metal, and ESAB OK Autrod 12.51 wire. A visual test (VT) was first performed on the welded specimens. The specimens were cut and polished to prepare for the conventional metallographic samples. The samples were evaluated by light optical microscopy and scanning electron microscope (SEM). Three types of cold laps were observed, i.e. spatter cold lap, overlap cold lap and spatter-overlap cold lap.

Spatter cold lap, named as type I, is formed when a spatter is situated close to the weld toe so that the spatter is fused and partially included in the weld. It is worth pointing out here that the cold laps from spatters stated in [12] can also be regarded as a specific situation in which the spatter is fully embedded in the weld and is invisible [12]. In this case, it can be characterized by L<-R if we regard the positive value in the direction away from the weld centre, as shown in Figure 22. The spatter cold lap is in a semicircle on the weld toe and the size depends on the size of spatter, which can range from several millimetres down to ten micron.

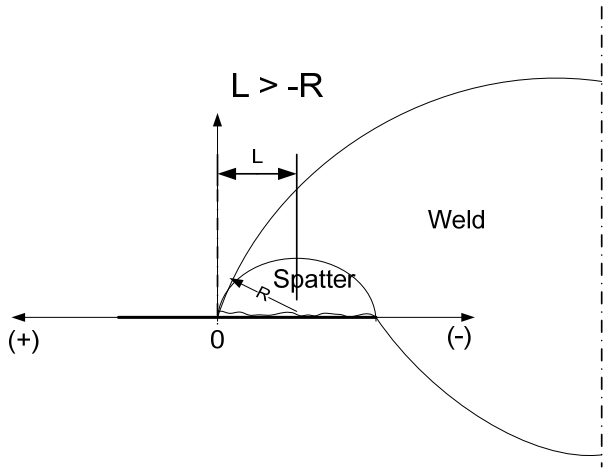

Figure 22 One specific situation of the spatter cold lap

Type II is named overlap cold lap, and is believed to be caused by a local overflow of the melted material in the weld pool in which the overflow metal incompletely fuses with the base metal on its surface. Overlap cold laps are usually semielliptical at the weld toe, which can be several millimetres in both longitudinal and transversal axes of the weld. It is also possible to

find cold laps along the entire weld toe (in the longitudinal direction of the weld), which are usually caused by the poor surface condition of the base metal and improper welding parameters. Type III is referred to as “spatter-overlap cold lap”, and can be regarded as a combination of type I and type II. This usually appears in a worm-like shape and can be several millimetres away from the weld toe.

Microscopy analysis of the spatter/base metal interface has revealed a lack of fusion consisting of both voids and oxides. The main oxides detected were Mn-Si oxides, which can be symbolised with the general formula $(Mn{\bullet}Si)O_n$ where n varies from 0.3 to 0.5.

6.2 Paper II

The main purpose of this paper is to investigate the influence of the Mn-Si oxides observed in paper I on cold laps. Secondly, any other influencing factors on cold laps were studied. A series of tandem arc welding experiments was performed in a sealed chamber filled up either with pure argon or with pure CO_2 with the purpose of creating oxidizing or non-oxidizing welding environments, respectively, and studying the influence of the shielding gas on the formation of cold laps. Two surface conditions, i.e. an iron sand blasted surface and a burr grinding surface, were prepared for the base metal. The welded specimens were visually examined using the naked eye. Spatters were also evaluated in terms of size and distribution on the welded specimens. In the pure Ar welding process, smaller spatters were generated and concentrated in a small area close to the weld toe, whereas the spatters in pure CO_2 welding were larger in size and more evenly distributed.

All three types of cold laps were identified and analysed. The interface of different types of cold laps was examined using a light optical microscope, SEM and EDS. Voids and Mn-Si oxides were found in the cold lap interface. The results revealed that the Mn-Si oxides have the most significant influence on overlap cold lap occurrence. It was also observed that the blasted surface can enhance the lack of fusion by easing the air entrapment in the interface. By evaluating the spatter surface and base metal surface after welding regarding Mn-Si oxides, it could be concluded that the Mn-Si oxides in cold laps came mainly from the oxidization of droplets before they reached the weld pool.

6.3 Paper III

The main purpose of this paper is to reveal the factor(s) behind the cold laps found in the pure Ar welding in paper II, by studying the spatter/base metal interface. The spatter/base metal interface was investigated for two different welding conditions, i.e. in pure Ar and in pure CO_2. The contribution of Mn-Si oxides was confirmed for the lack of fusion formation at the spatter/base metal interface. The ratio between the length of lack of fusion at the interface and the entire length of the spatter/base metal interface (RLoF) was introduced in this investigation. Studying the RLoF against spatter distance and spatter diameter revealed that the RLoF increased abruptly until the spatter diameter reached a critical value (approx. 1 mm) as the spatter diameter decreased from its highest value. For lower spatter diameter values than the critical value (i.e. under 1 mm), the RLoF remained constant (100%) with the continuous decrement of spatter diameter. A direct proportion was revealed between spatter distance and RLoF. However, the heat/temperature of the spatter is influenced by both the

spatter diameter and the spatter distance regarding the fusion between spatter and base metal. Therefore, the heat/temperature can be regarded as the other important influence factor for lack of fusion formation.

7 Conclusions and future work

Through the experimental study of cold laps, three types of cold laps were identified, i.e. overlap old lap, spatter cold lap, and spatter-overlap cold lap. For all types of cold laps, the interface was characterized by voids and oxides. The oxides depended on the welding consumables. For the materials applied in this study, manganese-silicon oxides were shown to have significant influence on cold lap occurrence. The influence of temperature on cold laps was shown by the indicators of spatter diameter and distance from spatter to the weld.

In the future work, the temperature influence of the welding workpiece on cold laps should be investigated. Also, the behaviour of the welding pool can be studied with help of high speed imaging technology. Regarding the influence of oxides on cold laps, new consumables of GMAW, which can avoid oxides in welding process, are of interest to study.

8 References

1. L.Lopez.Martinez, P.Korsgren. Characterization of Initial Defect Distribution and Weld Geometry in Welded Fatigue Test Specimens. In, Fatigue under spectrum loading and in corrosive environments. Denmark: EMAS; 1993
2. J.Samuelsson. Cold laps and weld quality acceptance limits. In: J.Samuelsson ed, Design and Analysis of Welded High Strength Steel Structures. Stockholm, Sweden: EMAS; 2002:151-161
3. Z.Barsoum, B.Jonsson. Fatigue assessment and LEFM analysis of cruciform joints fabricated with different welding processes. Welding in the world 2008;52:93-105
4. M.Lundin, L.Lopez.Martinez, J.Hedegård, K.Weman. High productive MAG welding - Fatigue properties of weldments. In, Welded High-Strength Steel Structures. Stockholm, Sweden: EMAS; 1997
5. L.Holst, M.Lundin, J.Hedegård, K.Weman. High productive MAG-Welding- Weld toe defects - A new detection method. In, Welded High-Strength Steel Structures. Stockholm, Sweden: EMAS; 1997
6. K.Weman, M.Lundin, J.Hedegård. High productive MAG welding of vehicle components. In, Welded High-Strength Steel Structures. Stockholm, Sweden: EMAS; 1997
7. Volvo weld quality standard. In, STD181-0004. Sweden; 2008
8. K.Weman. Welding Process Handbook: CRC Prss Inc (5 Aug 2003); 2003
9. R.L.O'Brien. WELDING PROCESS. Eighth ed. MIAMI: AMERICAN WELDING SOCIETY; 1995
10. Pritchard D. Soldering, Brazing & Welding-A Manual Of Techniques: The Crowood Press; 2001
11. L.P.Connor. WELDING TECHNOLOGY. Eighth ed. Miami: AMERICAN WELDING SOCIETY; 1987
12. M.Farajian-Sohi, N.Järvstråt. A Fractographical Investigation of Weld Toe Imperfections in Tandem Gas Metal Arc Welding. Steel research international 2006;77 (2006) No.12:889-895
13. J.Hedegård, L.Lopez.Martinez, N.Moradashkafti, H.Trogen. The influence of welding parameters on the size and distribution of weld defects for various weld methods. In, VTT Symposium 156:Fatigue Design 1995. Helsinki: VTT Offset print Espoo 1995; 1995
14. M.Farajian-Sohi, N.Järvstråt, M.Thuvander. Effect of Welding Parameters on Formation of Toe Imperfections in Tandem Gas Metal Arc Welding In, 7th International Conference on Trends in Welding Research. Geogia, USA: ASM; 2005
15. L.Lopez.Martinez, A.F.Blom, J.Samuelsson. Weld defects before and after post weld treatment for MAG and high-productivity MAG welding. In, Welded High-Strength Steel Structures. Stockholm, Sweden: EMAS; 1997
16. G.E.Linnert. Welding Metallurgy. Hilton Head Island, South Carolina: AWS; 1994
17. E.T.Turkdogan. Deoxidation of steel. In, Chem Metall of Iron and Steel. Sheffield, U.K.: The Iron and Steel Institution; 1973:153-170
18. O.Grong, N.Christensen. Factors Controlling MIG Weld Metal Chemistry. Scandinavian Journal of Metallurgy 1983;12:155-165
19. SSAB. Domex 355 MC Datablad. In. Brolänge: SSAB; 2011

9 Appended papers